THE JOURNAL OF BIOLOGICAL CHEMISTRY VOL. 283, NO. 12, pp. 7705–7712, March 21, 2008

Structural Insights into Mechanisms of Catalysis and Inhibition in Norwalk Virus Polymerase*

Received for publication, November 21, 2007, and in revised form, December 13, 2007 Published, JBC Papers in Press, January 9, 2008, DOI 10.1074/jbc.M709563200

Dmitry F. Zamyatkin[‡], Francisco Parra[§], José M. Martín Alonso[§1], Daniel A. Harki[¶2], Blake R. Peterson[¶], Pawel Grochulski[‖], and Kenneth K.-S. Ng[‡3]

From the [‡]Department of Biological Sciences and Alberta Ingenuity Centre for Carbohydrate Science, University of Calgary, Calgary, Alberta T2N 1N4, Canada, the [§]Departamento de Bioquímica y Biología Molecular, Instituto Universitario de Biotecnología de Asturias, Universidad de Oviedo, 33006 Oviedo, Spain, the [¶]Department of Chemistry, The Pennsylvania State University, University Park, Pennsylvania, 16802, and the [‖]Canadian Light Source, Inc., University of Saskatchewan, Saskatoon, Saskatchewan S7N 0X4, Canada

Crystal structures of Norwalk virus polymerase bound to an RNA primer-template duplex and either the natural substrate CTP or the inhibitor 5-nitrocytidine triphosphate have been determined to 1.8 Å resolution. These structures reveal a closed conformation of the polymerase that differs significantly from previously determined open structures of calicivirus and picornavirus polymerases. These closed complexes are trapped immediately prior to the nucleotidyl transfer reaction, with the triphosphate group of the nucleotide bound to two manganese ions at the active site, poised for reaction to the 3′-hydroxyl group of the RNA primer. The positioning of the 5-nitrocytidine triphosphate nitro group between the α-phosphate and the 3′-hydroxyl group of the primer suggests a novel, general approach for the design of antiviral compounds mimicking natural nucleosides and nucleotides.

Norwalk virus (NV)[4] is the prototype species of the *Norovirus* genus within the *Caliciviridae* and is a major cause of gastroenteritis outbreaks in developed countries (1). Unfortunately, effective treatments are not currently available for many important diseases caused by NV and related RNA viruses. The virally encoded RNA-dependent RNA polymerase (RdRP) is the central enzyme required for replication (2) and is one of the key targets for the development of novel antiviral agents. Recently, 5-nitrocytidine triphosphate (NCT) was identified as a potent inhibitor of picornaviral polymerases, and the nucleoside 5-nitrocytidine was found to have low toxicity and significant antiviral activity in a cultured cell viral infection model (3). A structural and mechanistic basis for rationalizing the inhibitory activity of NCT and related inhibitors is currently lacking because of a shortage of high resolution structural information on RdRP replication complexes.

Details on the structure and mechanism of viral RdRPs are clearly required to understand the replication of RNA viruses and to develop more effective antiviral agents. Previous structural studies of viral RdRPs from positive strand RNA viruses and double-strand RNA viruses indicate that the general features of RdRP architecture are highly conserved throughout a diverse range of viruses (reviewed in Refs. 2 and 4). The three-dimensional arrangement of N-terminal, fingers, palm, and thumb domains, as well as the active site residues in motifs A–F are nearly universally shared (5).

The structural conservation seen in RdRPs suggests that the enzymatic mechanism of nucleotidyl transfer is also highly conserved. Studies primarily on poliovirus RdRP have revealed many of the basic features underlying the nucleotidyl transfer reaction in RdRPs (6, 7). These studies and others indicate that RdRPs, like other polynucleotide polymerases, follow a five-step reaction cycle involving (i) the binding of an NTP complementary to the base of the template to form an initial "open" complex, followed by (ii) a conformational change to the "closed" complex, (iii) nucleotidyl transfer and translocation, (iv) a second conformational change, and finally (v) the release of pyrophosphate (see Fig. 1). Experimentally determined structural information is clearly needed to corroborate and further elaborate the different states identified from kinetic studies, but trapping these different states has proven to be very challenging in RdRPs and other polymerases. Crystal structures of RdRP·RNA·NTP complexes from reovirus (8) and foot-and-mouth disease virus (FMDV) (9) have revealed important aspects of RNA and NTP binding, but key details of the closed

* This work was supported in part by Natural Sciences and Engineering Research Council (NSERC), National Research Council, Canadian Institutes of Health Research, the University of Saskatchewan, the Alberta Synchrotron Institute, the National Institutes of Health, the National Science Foundation, the University of California and Henry Wheeler, the Alberta Science and Research Authority, and Alberta Heritage Foundation for Medical Research (AHFMR). This work was supported by NSERC Discovery Grant 262089 and Canadian Institutes of Health Research Operating Grant MOP-67209 (to K. N.), National Institutes of Health Grant AI054776 (to B. R. P.), and Grant BIO2006-00827 from the Spanish Ministerio de Educación y Ciencia cofinanced by Fondo Europeo de Desarrollo Regional (to F. P.). The costs of publication of this article were defrayed in part by the payment of page charges. This article must therefore be hereby marked "*advertisement*" in accordance with 18 U.S.C. Section 1734 solely to indicate this fact.

The atomic coordinates and structure factors (code 3BSN and 3BSO) have been deposited in the Protein Data Bank, Research Collaboratory for Structural Bioinformatics, Rutgers University, New Brunswick, NJ (http://www.rcsb.org/).

[1] Recipient of a "Ramón y Cajal" contract from the Spanish Ministerio de Educación y Ciencia cofinanced by Fondo Social Europeo.

[2] Supported by a predoctoral fellowship from the American Heart Association.

[3] Canadian Institutes of Health Research New Investigator and AHFMR Senior Scholar. To whom correspondence should be addressed: Dept. of Biological Sciences, University of Calgary, 2500 University Dr. N.W., Calgary, Alberta T2N 1N4, Canada. Tel.: 403-220-4320; Fax: 403-289-9311; E-mail: ngk@ucalgary.ca.

[4] The abbreviations used are: NV, Norwalk virus; FMDV, foot-and-mouth disease virus; HIV, human immunodeficiency virus; NCT, 5-nitrocytidine triphosphate; RdRP, RNA-dependent RNA polymerase; DTT, dithiothreitol; CHAPS, 3-[(3-cholamidopropyl)dimethylammonio]-1-propanesulfonic acid.

catalytic complex formed in step iii remain poorly determined. The reovirus RdRP·RNA·GTP initiation complex (Protein Data Bank code 1N1H) contains two divalent metal ions at the active site and the NTP bound near the RNA primer terminus. Unfortunately, the 2.8-Å diffraction limit prevents a detailed analysis of molecular conformation, hydrogen bonding, and water structure at the active site. The FMDV structures were determined at a similar resolution (2.5–3.0 Å) and appear to be open complexes trapped at steps ii or v. The NTP is bound too far from the primer terminus for the nucleotidyl transfer reaction to occur in the open complexes, and one of the two divalent metal ions needed for the two-metal ion mechanism of catalysis (10) is missing from the active site.

To provide a more detailed structural basis for understanding the nucleotidyl transfer reaction in viral RdRPs, we have determined high resolution structures of NV RdRP bound to a self-complementary oligonucleotide (5′-UGCCCGGG-3′), two Mn^{2+} ions, and either the natural substrate CTP or the nucleotide inhibitor NCT. These structures reveal for the first time details of ternary RdRP·RNA·NTP complexes trapped immediately prior to the nucleotidyl transfer reaction (the closed *complex iii* in Fig. 1*A*). Comparisons of the structures of the CTP and NCT complexes also suggest a novel mechanism for inhibition that may be exploited for the design of more effective antiviral agents.

EXPERIMENTAL PROCEDURES

Synthesis of 5-Nitrocytidine Triphosphate (NCT) and RNA—NCT was synthesized as previously described (3). The 5′-UGCCCGGG-3′ sequence was synthesized by the University of Calgary Core DNA Services facility (University of Calgary). The desalted oligonucleotide was dissolved at a concentration of 3.5 mM RNA duplex (7 mM single-stranded RNA) in 1 mM sodium citrate, pH 6.2, 50 mM potassium chloride. To anneal the self-complementary oligonucleotide into a duplex form, the oligonucleotide was heated to 80 °C and cooled at the rate of 5 °C/min using a thermocycler.

Expression and Purification of NV Polymerase—NV polymerase was expressed and purified as previously described (11), except for the following modifications. 1-Liter cultures of *Escherichia coli* XL1-Blue transformed with pGEX-NV-3D were induced with 0.2 mM isopropyl-β-D-thiogalactoside and then grown at 25 °C for 20 h. The cells were harvested by centrifugation and resuspended in 30 ml of buffer A (50 mM Tris-Cl, pH 8.0, 150 mM NaCl, 0.25 mM EDTA). The cells were lysed by sonication in the presence of lysozyme and DNase I. The concentration of sodium chloride was then raised to 0.3 M, and polyethylenimine (Sigma) was added dropwise to a final concentration of 0.1% (w/v) to help remove nucleic acids. The extract was clarified by centrifugation and loaded sequentially onto two 2-ml columns of glutathione-Sepharose 4B (GE Healthcare) equilibrated in buffer B (20 mM Tris-Cl, 450 mM NaCl, 1 mM EDTA, 4 mM DTT). The columns were washed with 50 ml buffer of B and 20 ml of buffer C (25 mM Na-HEPES, pH 7.5, 100 mM NaCl, 0.5 mM EDTA, 4 mM DTT, and 10% glycerol). Thrombin (20 units, GE Healthcare) was diluted into 1 ml of buffer C and incubated for 90 min with each of the two 2-ml columns of glutathione-Sepharose. Each column was eluted with 10 ml of buffer C, and the thrombin was inactivated with 0.5 mM 4-(2-aminoethyl) benzenesulfonyl fluoride. The digestion was repeated for each column, and all of the eluates were pooled. The pooled eluates were dialyzed overnight against 1 liter of buffer D (25 mM Na-HEPES, pH 7.0, 25 mM of NaCl, 0.5 mM EDTA, 4 mM DTT, and 15% glycerol) and then loaded onto a 5-ml HiTrap SP-Sepharose column. The column was washed with 30 ml of buffer D containing 30 mM NaCl, and NV polymerase was eluted with an 80-ml linear gradient of buffer D containing 30–150 mM NaCl. Peak fractions were diluted with RNase-free buffer E (25 mM Tris-HCl, pH 8.0, and 15% glycerol (Fluka)) to reduce the NaCl concentration to 20 mM and loaded onto a Sartobind Q15F filter (Sartorius). The filter was washed with buffer E and eluted with RNase-free buffer F (10 mM Tris, pH 8.0, 300 mM NaCl, 6 mM DTT, and 15% glycerol). NV polymerase was diluted into buffer G (10 mM Tris, pH 8.0, 150 mM NaCl, 6 mM DTT, and 15% glycerol) and concentrated with an Amicon Ultrafree-4 (10,000 molecular weight cut-off) centrifugal filter to 7.5 mg/ml (0.13 mM, concentration estimated by UV absorption using a calculated extinction coefficient of 1.43 OD/(mg/ml)). NV polymerase was filtered with a 0.22-μm Spin-X cellulose acetate centrifugal filter (Costar) and stored on ice.

Crystallization—CHAPS (0.2% w/v) and Superase-In ribonuclease inhibitor (1 unit/μl; Ambion) were added to NV polymerase prior to crystallization. The annealed RNA duplex (18 μl) was mixed with 4.5 μl of NCT or CTP (25 mM) and 31.5 μl water to prepare a mixture containing 1.16 mM RNA duplex and 2.1 mM NTP. A reservoir solution containing 16% polyethylene glycol 8000, 25% glycerol, 100 mM Tris-HCl, pH 7.0, 50 mM KCl, 4 mM $MgCl_2$, 10 mM $MnCl_2$, and 0.1% 2-mercaptoethanol was prepared.

Reservoir solution (3 μl) was mixed with the RNA-NTP mixture (6 μl) and NV polymerase (4 μl). This mixture was suspended as a hanging drop and equilibrated against 1 ml of reservoir solution at 22 °C. Crystals appeared within a week and grew to full size (~0.2 × 0.1 × 0.05 mm) after 2–3 weeks.

Crystal Structure Determination—A single crystal (0.2 × 0.1 × 0.05 mm) grown in the presence of NCT was quickly mounted in a polymer fiber loop (Hampton Research) and flash-cooled in a nitrogen gas stream at ~100 K. Diffraction data were initially measured using a MAR 345 image plate and X-rays produced with a rotating copper anode (Rigaku RUH3R). The crystal was stored in liquid nitrogen and transferred to the Canadian Light Source beamline 08ID-1 for data collection using a Marmosaic CCD225 detector. The data were processed and scaled using XDS (12) (data quality and refinement statistics are given in Table 1). The structure of unliganded NV polymerase (Protein Data Bank code 1SH0) was used as the search model for molecular replacement calculations using PHASER (13). Very clear solutions were obtained for the rotational (z = 20.8) and translational (z = 26.3) placement of a single polymerase molecule, yielding a solvent content of 59% and V_m = 3.0. Initial electron density maps clearly indicated that an RNA duplex, metal ions, and NTP were present. Initial maps also showed that the C-terminal segment was missing and that residues 437–452 in the thumb domain needed to be rebuilt. A model for the RNA segment was built with reference

TABLE 1
Crystallographic statistics

	NCT complex (3BSN)	CTP complex (3BSO)
Data collection		
Space group	$P2_12_12_1$	$P2_12_12_1$
Unit cell lengths (Å)	a = 74.3, b = 93.9, c = 96.0 Å	a = 75.1, b = 93.5, c = 96.5 Å
Wavelength (Å)	0.97934	1.11587
Resolution (Å)	30-1.8	40-1.74
High resolution (Å)	1.97-1.80	1.80-1.74
Total reflections[a]	283615 (49434)	262319 (19967)
Unique reflections[a]	58959 (11566)	69074 (6276)
Completeness (%)[a]	93.6 (78.3)	98.1 (90.5)
I/σ[a]	13.7 (2.3)	29.2 (2.0)
R_{sym}[a,b]	0.079 (0.614)	0.045 (0.436)
Refinement		
R_{work}[c]	0.201 (0.314)	0.201 (0.258)
R_{free}[d]	0.236 (0.360)	0.232 (0.301)
Number of atoms		
Protein	3762	3762
RNA + NTP	393	373
Solvent and Ions	374	422
Root mean square deviations from ideal geometry		
Bond lengths (Å)	0.006	0.007
Bond angles (°)	1.00	1.06
Average temperature factors (Å^2)		
Wilson plot	24.8	34.8
Protein	30.1	37.7
RNA	31.1	39.5
Water	36.8	44.6
Ramachandran plot (% in regions defined by Procheck (18))		
Most favored	94.1	92.6
Additional allowed	5.9	7.2
Generously allowed	0.0	0.2
Disallowed	0.0	0.0

[a] The values from the outermost resolution shell are given in parentheses.
[b] $\Sigma_h\Sigma_i(|I_i(h) - <I(h)>|)/\Sigma_h\Sigma_i I_i(h)$, where $I_i(h)$ is the i^{th} integrated intensity of a given reflection and $<I(h)>$ is the weighted mean of all measurements of $I(h)$.
[c] $\Sigma_h||F(h)_o| - |F(h)_c||/\Sigma_h|F(h)_o|$ for the 95% of reflection data used in refinement.
[d] $\Sigma_h||F(h)_o| - |F(h)_c||/\Sigma_h|F(h)_o|$ for the 5% of reflection data excluded from refinement.

to the FMDV·RNA complexes and high resolution RNA helices deposited in the NDB. Coot (14) and MI-Fit (15) were used for model building, and Refmac (16) was used for refinement. The electron density maps clearly showed the incorporation of a single NCT residue in the distal end of the primer-template duplex bound to NV RdRP. This residue must have been added by the polymerase onto this end of the primer, and the extended primer-template duplex must have dissociated from the enzyme before it rebound NV RdRP and crystallized. At the conclusion of refinement, residues 1–4, 467–471, and 489–510 were not modeled, presumably because of the presence of disorder.

Diffraction data were also measured for a crystal (0.3 × 0.15 × 0.08 mm) grown in the presence of CTP and flash-cooled to ~100 K as described for the NCT complex. A complete data set was initially measured using the laboratory Mar345 image plate detector and rotating copper anode x-ray generator (Rigaku RUH3R) before the crystal was transferred to the Advanced Light Source beamline 8.3.1 for data collection using an ADSC Q-315 detector. The data were processed and scaled using the HKL Suite (17). The refined structure of the NCT complex was used as a starting model for the refinement of the CTP complex. The nitro group of the bound nucleotide and the nitro group of the nucleotide incorporated into the distal end of the primer-template duplex were removed from the model, because these moieties were clearly absent in electron density maps. The quality of geometric parameters was evaluated by Procheck (18).

RESULTS

Overall Structure of NV RdRP·RNA·NTP Complexes—Ternary complexes of NV RdRP reveal an RNA primer-template duplex and NTP bound in the active site cleft (Figs. 1*B* and 2). As predicted previously, RNA binding displaces the C-terminal tail from the active site cleft of NV RdRP (11). Residues 489–516 are not defined by electron density, suggesting that the C-terminal tail is unstructured. The binding of RNA also causes the central helix of the thumb domain (residues 435–449) to rotate by 22°, thus inducing the formation of a binding groove for the primer strand (Fig. 2). The rotation of this helix appears to be coupled to the movement of the C-terminal tail away from the active site cleft. In the unbound conformation of NV and Sapovirus RdRPs, the proximal portion of the C-terminal tail (residues 489–502 in NV) packs against this central helix, acting as a brace to resist the outward rotation of the helix seen in the RNA-bound conformation (11, 19). The movement of the C-terminal tail away from the active site cleft allows the central helix the room to rotate and interact with the primer strand and minor groove of the primer-template duplex.

These conformational changes are reminiscent of changes seen in DNA polymerases following the binding of DNA and dNTPs (20) and are larger than the conformational changes previously seen in viral RdRPs crystallized in different packing environments (21, 22) or bound to allosteric inhibitors (23). The conformational changes seen in the NV RdRP·RNA·NTP complex are also much larger than the changes seen in the FMDV RdRP·RNA·NTP complexes, in which the conformation

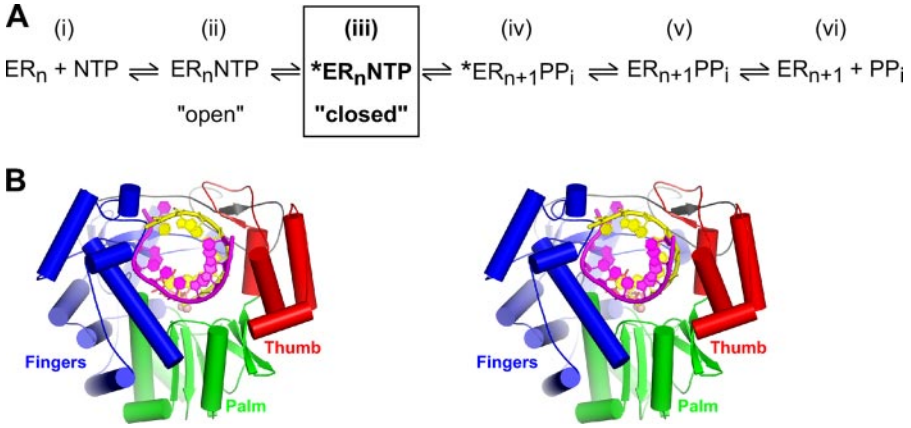

FIGURE 1. *A*, general kinetic scheme for nucleotide incorporation in RdRPs and other polymerases (36, 37). *E*, RdRP enzyme; R_n, RNA oligonucleotide containing *n* nucleotides; R_{n+1}, RNA oligonucleotide containing $n + 1$ nucleotides; *NTP*, nucleoside triphosphate; PP_i pyrophosphate. *B*, stereoscopic view of the NV RdRP·ERnNTP complex with the primer RNA strand colored *yellow*, template RNA strand in *magenta*, fingers domain in *blue*, palm domain in *green*, and thumb domain in *red*.

of the RdRP is nearly identical to the unbound form (9). This observation, in combination with the modes of binding observed for divalent metal cations and NTPs in the FMDV complexes, further suggest that the NV RdRP·RNA·NTP complex is a closed complex trapped immediately prior to catalysis, whereas the FMDV complexes are open complexes trapped at earlier or later steps of the reaction cycle.

Interactions between RdRP, RNA, NTPs, and Metal Ions at the Active Site—The structures of the NV RdRP NCT and CTP complexes provide the first high resolution views of RdRP complexes trapped immediately before nucleotidyl transfer. Indirect effects from crystal packing appear to have fortuitously trapped these complexes at this stage of the reaction cycle. The distal end of the primer-template duplex is located near a symmetry-related polymerase molecule, and there is insufficient space for primer extension to occur in this crystal form. As a result, polymerase molecules in this crystal form bind substrates and assemble active complexes that can only proceed up to the point immediately prior to nucleotidyl transfer.

The intricate network of interactions surrounding the bound nucleotide reveals at high resolution several key elements underlying substrate binding and catalysis in RdRPs (Fig. 3). The NTP bases form hydrogen bonds with the complementary guanosine base of the template and stack against the 3′-terminal base of the primer, as well as the Arg-182 guanidino group (Fig. 3). Arg-182 is highly conserved in RdRPs (Motif F3) (5) and is near the NTP α-phosphate (3.5 Å). Arg residues occupy a similar position in all viral RdRPs with known structures, as well as distantly related enzymes like HIV reverse transcriptase (Table 2). The cytosine and nitrocytosine bases stack tightly against Arg-182, unlike the looser interactions seen in the more open FMDV complexes (9).

The interactions made by the ribose and triphosphate moieties of the bound nucleotide indicate that the NV RdRP complexes are perfectly positioned for nucleotidyl transfer (Fig. 3). The 2′-OH accepts a hydrogen bond from Asn-309 and donates a hydrogen bond to Ser-300, which in turn donates a hydrogen bond to Asp-247. This pattern of hydrogen bonding reveals how these highly conserved residues (equivalent to poliovirus RdRP residues 297, 288, and 238, respectively) distinguish ribonucleotides from 2′-deoxyribonucleotides (24–26). A similar network of hydrogen bonds is seen in one of the reovirus·NTP·RNA complexes (8), but the more open FMDV complexes or binary poliovirus RdRP·NTP complexes do not form the same hydrogen-bonding pattern, suggesting that ribonucleotide selection occurs in the closed complex formed immediately before catalysis (9, 27).

Two Mn^{2+} ions also coordinate to three highly conserved Asp residues and the NTP triphosphate moiety to mediate catalysis through the two-metal-ion mechanism (10, 28) (Fig. 3). Metal ion A octahedrally coordinates to the 3′-OH nucleophile of the primer, the NTP α-phosphate, the carboxylate groups of Asp-242, Asp-343, and Asp-344, as well as a water molecule. By donating hydrogen bonds to the negatively charged primer phosphodiester and NTP α-phosphate groups, this water molecule may be activated to become a better general base catalyst (7), thus allowing it to abstract a proton from the primer 3′-OH (2.8 Å away) following a mechanism similar to that proposed for DNA polymerase β (29, 30). Metal ion B also octahedrally coordinates to the side chain carboxylate groups of Asp-242 and Asp-343, the main chain carbonyl group of Tyr-243, as well as a single oxygen atom from each of the α, β, and γ phosphate groups of the NTP.

DISCUSSION

Trapping of a Preinsertion Conformation of NV RdRP via Constraints from Crystal Packing—The recombinant form of NV RdRP used in these studies is enzymatically active (11), and there is surprisingly clear evidence of this activity in the crystal structure itself. Because the primer-template oligonucleotide is self-complementary and symmetrical, each oligonucleotide duplex contains two 5′-overhangs where primer extension can occur. In the NV RdRP·RNA·NTP complexes, the end of the duplex found in the enzyme active site reveals the presence of a 3′-terminal guanosine residue in the primer and a 3′-GU-5′ sequence for the single-stranded 5′-overhang of the template strand. CTP or NCT forms a Watson-Crick base pair with the guanosine residue of the template, but crystal packing interactions at the distal end of the primer-template duplex appear to impede the translocation event following nucleotidyl transfer, thus trapping this complex. Surprisingly, the end of the primer-template duplex that is located distal from the active site reveals that either a cytidine or 5-nitrocytidine residue has been added to the primer strand, presumably prior to crystallization. This residue must have been added when this end of the duplex was bound at the active site. Following the addition of this single residue, the duplex must have dissociated from the enzyme and bound in the opposite orientation prior to crystallization.

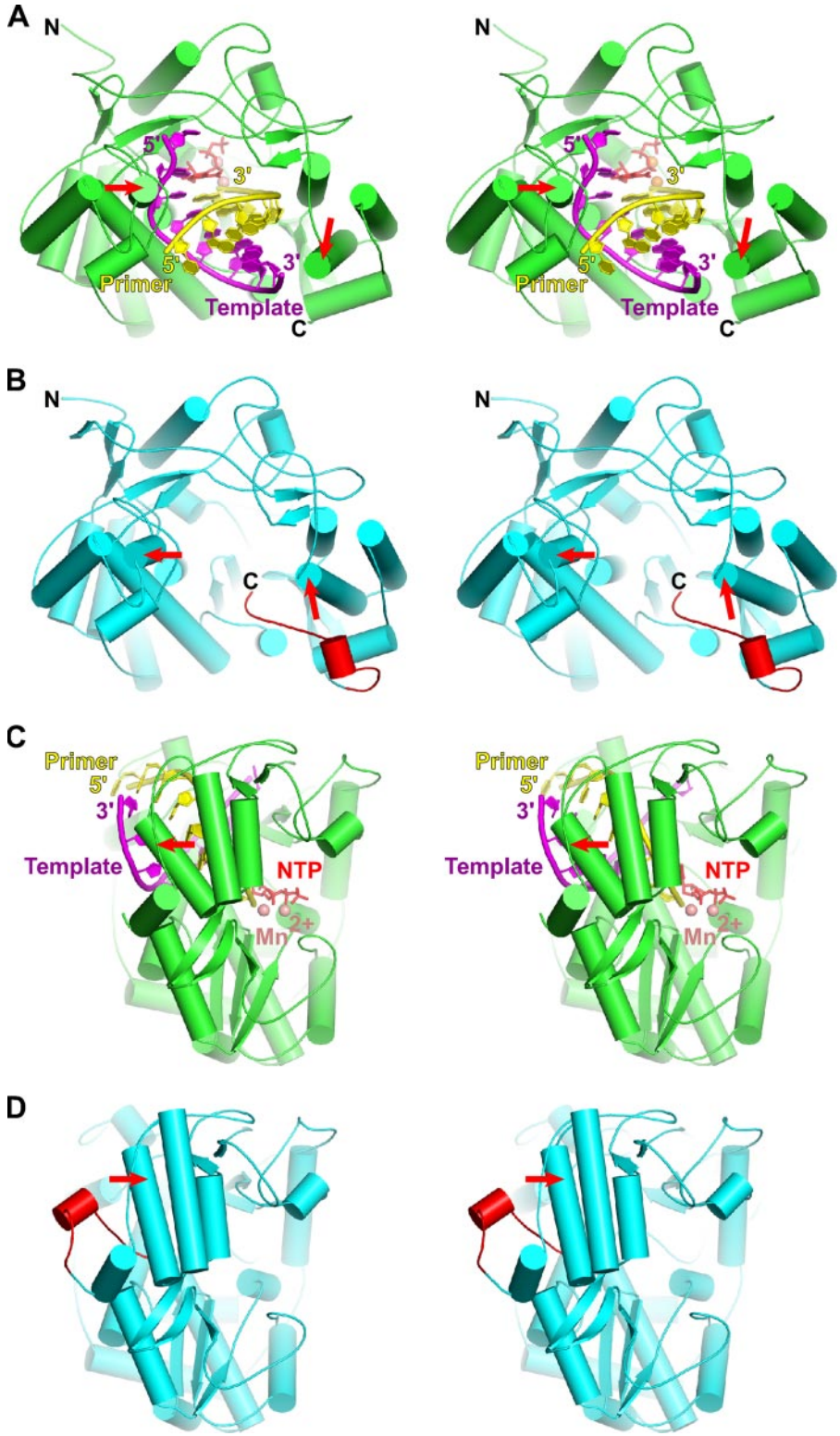

FIGURE 2. **Stereoscopic overall views of (*A*, top; *C*, side) NV RdRP·RNA·Mn^{2+}·NCT complex and (*B*, top; *D*, side) uncomplexed NV RdRP (Protein Data Bank code 1SH0 (11)).** The primer (*yellow*) and template (*magenta*) strands of RNA, NCT (*red*), and Mn^{2+} (*pink*) are drawn. The C-terminal tail of unbound NV RdRP is highlighted in *red*. The largest conformational changes in the thumb and fingers domains following the binding of RNA are highlighted with *arrows*.

The packing arrangement of molecules in this crystal form appears to be critical for arresting the normal reaction cycle of NV RdRP at the point immediately prior to nucleotidyl transfer. Previous studies on a wide range of polynucleotide polymerases indicate the necessity of a translocation step immediately following nucleotidyl transfer (20). All of the previously determined crystal structures of polymerases trapped at this pre-insertion step of the reaction cycle have been chemically trapped by the use of substrate analogues like primer strands missing the 3′-hydroxyl group or a nucleoside 5′-(α,β)-imidotriphosphate analogue (29, 31–35). Such complexes provide a valuable but slightly distorted view of the natural complex. The fortuitous molecular packing arrangement in the NV RdRP·RNA·NTP crystal form has allowed us to trap a critical intermediate in the reaction cycle without introducing distortions through chemical modifications. The most similar, active polymerase complex for which a high resolution structure has been previously determined is the DNA polymerase β·DNA·2′-deoxyuridine-5′-[(α,β)-imido]triphosphate complex determined to 1.65 Å resolution (29). The trapped catalytic complex seen in DNA polymerase β closely resembles the NV RdRP ternary complex, including the presence of water molecules that may participate in catalysis.

A Novel and General Mechanism of RdRP Inhibition by NCT—The structure of the NCT complex suggests a novel mechanism of inhibition. The nitro group is 2.7 Å from the NCT α-phosphate and 4.3 Å from the 3′-OH nucleophile of the primer. If the pentavalent transition state forms halfway between the ground state positions of the 3′-OH nucleophile and the α-phosphate electrophile, the proximity of the negatively charged nitro group (~3 Å) to the negatively charged oxygen atoms of the transition state could destabilize the transition state of the nucleotidyl transfer reaction. The stacking of Arg-182 and the 3′-end of the primer against the NTP base, as well as base-pairing interactions with the template strand all act to fix the position of the NTP base, thus keeping the nitro group close to the negatively charged transition state. Finally, the nitro group displaces a water molecule that forms hydrogen bonds

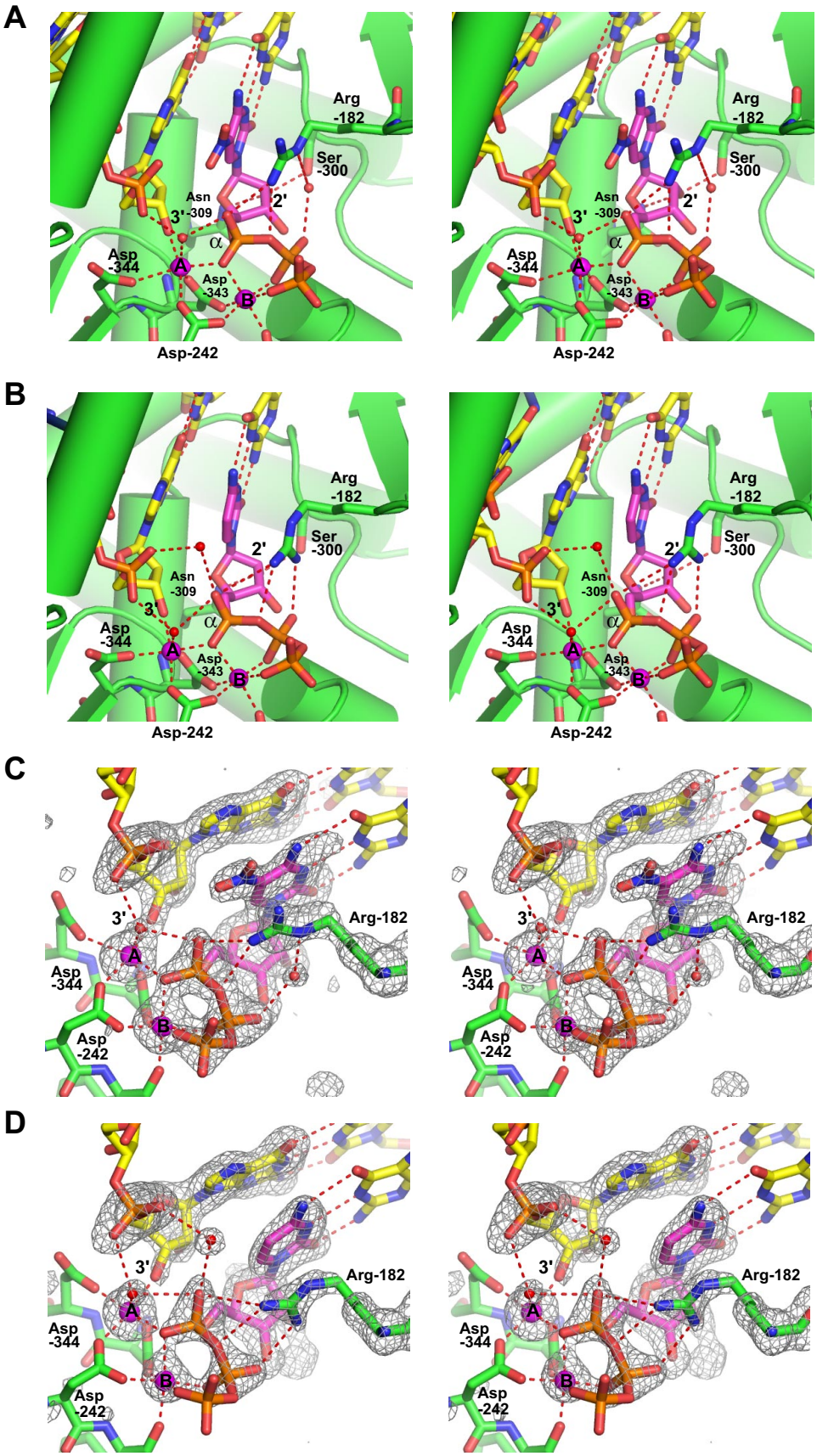

FIGURE 3. **Stereoscopic views of the active site of the NCT (*A* and *C*) and CTP (*B* and *D*) complexes.** In *panels A* and *B*, coordination bonds (*red dashes*) with Mn^{2+} ions A and B (*pink spheres*), and hydrogen bonds (*red dashes*) between the bound nucleotide (*magenta*), key water molecules (*red spheres*), and the protein are drawn. In *panels C* and *D*, Arg-182, the bound nucleotide, Mn^{2+} ions, and the terminal nucleotide of the primer were removed prior to 20 rounds of refinement and ($|F_o| - |F_c|$) electron density map calculation (3 σ contour). Figs. 2 and 3 were prepared using PyMOL (38).

TABLE 2
Motif F3 in RdRPs and HIV reverse transcriptase with known three-dimensional structures

Virus	Genome	Family	Protein Data Bank code	Start	End	F3 motif
NV	ssRNA(+)	*Caliciviridae*	1SH0	179	184	IKK**R**LL
RHDV	ssRNA(+)	*Caliciviridae*	1KHW	185	190	GKK**R**LL
SV	ssRNA(+)	*Caliciviridae*	2CKW	179	184	GKR**R**LL
PV	ssRNA(+)	*Picornaviridae*	2IM0	171	176	GKS**R**LI
HRV	ssRNA(+)	*Picornaviridae*	1TP7	171	176	GKT**R**VI
FMDV	ssRNA(+)	*Picornaviridae*	1U09	176	181	GKT**R**IV
HCV	ssRNA(+)	*Flaviviridae*	1CSJ	155	160	KPA**R**LI
DENV	ssRNA(+)	*Flaviviridae*	2J7U	203	208	KGS**R**AI
WNV	ssRNA(+)	*Flaviviridae*	2HCN	161	166	KGS**R**AI
BVDV	ssRNA(+)	*Flaviviridae*	1S48	212	217	KRP**R**VI
IBDV	dsRNA	*Birnaviridae*	2PGG	302	307	TKT**R**NI
Phi6	dsRNA	*Cystoviridae*	1HHS	267	272	ERR**R**TA
Reovirus	dsRNA	*Reoviridae*	1N35	523	528	RRP**R**SI
HIV	ssRNA-RT(+)	*Retroviridae*	1RTD	69	74	TKW**R**KL

with the α-phosphate of CTP and the 3′-terminal phosphodiester of the primer in the ground state. Loss of this water molecule in the NCT complex could further destabilize the transition state by reducing hydration.

Apart from the positioning of the nitro group and displacement of a water molecule from the vicinity of the reaction pathway, there are a few additional differences between the CTP and NCT complexes that may also contribute to the mechanism of inhibition of NCT. One important difference is a longer than expected coordination distance of 2.6 Å between Asp-344 and metal ion A in the NCT complex, when compared with the expected distance of 2.1 Å seen in the CTP complex (Fig. 3). The structures of the two complexes do not indicate a direct connection between the presence of the nitro group of NCT and effects on metal ion coordination. If this altered coordination geometry is an indirect effect of the nitro group from NCT, however, then this longer coordination distance may be related to an impairment of the nucleotidyl transfer reaction.

A second difference between the NCT and CTP complexes is the positioning of the side chain of Arg-182 (Fig. 3). The χ_4 torsion angle of Arg-182 differs by 180° between the conformation adopted in the NCT and CTP complexes. As a result, the conformation adopted in the NCT complex appears to form better π-stacking and electrostatic interactions with the nitro group (Fig. 3). The guanidino group of the side chain in both complexes forms good stacking interactions with the central portion of the base. Because the guanidino group is closer to the nitro group in the NCT complex, however, this group is farther from the β-phosphate than in the CTP complex. As a result, the Nϵ atom of Arg-182 forms a water-mediated hydrogen bond with the β-phosphate in the NCT complex, and one of the terminal nitrogen atoms forms a direct hydrogen bond with the oxygen atom bridging the α- and β-phosphates. In the CTP complex, however, the two terminal nitrogen atoms of Arg-182 form direct hydrogen bonds with the oxygen atom bridging the α- and β-phosphates, as well as a nonbridging oxygen atom on the β-phosphate. By altering the position of the guanidino group relative to the triphosphate moiety, the 5-nitro group may reduce the ability of Arg-182 to stabilize the pyrophosphate leaving group during the course of nucleotidyl transfer.

The mechanism of inhibition suggested by the structure of the NCT complex provides a general, new approach for inhibitor design. Large, negatively charged substituents at the 5- and 6-positions of pyrimidine bases may be effective at destabilizing the transition state without disturbing essential substrate binding interactions. Effective inhibitors should preserve favorable π-stacking and electrostatic interactions with the primer and Arg-182, as well as base pairing with the template. Substituents like the 5-nitro group that interact well with Arg-182 may bind viral RdRPs more effectively than host polymerases, because Arg is almost universally conserved at this position in viral RdRPs, but Arg is not conserved at this position in any of the family A, B, and Y DNA polymerases, eukaryotic RdRPs, and phage, prokaryotic, and eukaryotic DNA-dependent RNA polymerases. A neutral aromatic residue seems to occupy this position in most other polymerases.

The NV RdRP·RNA·NTP complexes reveal for the first time several structural features underlying the nucleotidyl transfer reaction that may be exploited for developing novel antiviral inhibitors. The synthesis and evaluation of novel inhibitors will provide powerful and practical tests for the mechanisms proposed in this paper.

Acknowledgments—We thank Dr. Isabelle Barrette-Ng for helpful discussions. We appreciate the support of the University of Calgary Core DNA Services oligonucleotide synthesis facility in providing us with the wide range of high quality RNA oligonucleotides required for this study and preliminary work.

REFERENCES

1. Blanton, L. H., Adams, S. M., Beard, R. S., Wei, G., Bulens, S. N., Widdowson, M. A., Glass, R. I., and Monroe, S. S. (2006) *J. Infect. Dis.* **193,** 413–421
2. Ortin, J., and Parra, F. (2006) *Annu. Rev. Microbiol.* **60,** 305–326
3. Harki, D. A., Graci, J. D., Galarraga, J. E., Chain, W. J., Cameron, C. E., and Peterson, B. R. (2006) *J. Med. Chem.* **49,** 6166–6169
4. Ferrer-Orta, C., Arias, A., Escarmis, C., and Verdaguer, N. (2006) *Curr. Opin. Struct. Biol.* **16,** 27–34
5. Bruenn, J. A. (2003) *Nucleic Acids Res.* **31,** 1821–1829
6. Cameron, C. E., Gohara, D. W., and Arnold, J. J. (2002) in *Molecular Biology of Picornaviruses* (Semler, B., and Wimmer, E., eds) pp. 255–267 ASM Press, Washington, DC
7. Castro, C., Smidansky, E., Maksimchuk, K. R., Arnold, J. J., Korneeva, V. S., Gotte, M., Konigsberg, W., and Cameron, C. E. (2007) *Proc. Natl. Acad. Sci. U. S. A.* **104,** 4267–4272
8. Tao, Y., Farsetta, D. L., Nibert, M. L., and Harrison, S. C. (2002) *Cell* **111,** 733–745
9. Ferrer-Orta, C., Arias, A., Perez-Luque, R., Escarmis, C., Domingo, E., and Verdaguer, N. (2007) *Proc. Natl. Acad. Sci. U. S. A.* **104,** 9463–9468

10. Steitz, T. A. (1998) *Nature* **391,** 231–232
11. Ng, K. K., Pendas-Franco, N., Rojo, J., Boga, J. A., Machin, A., Alonso, J. M., and Parra, F. (2004) *J. Biol. Chem.* **279,** 16638–16645
12. Kabsch, W. (1993) *J. Appl. Crystallogr.* **26,** 795–800
13. Read, R. J. (2001) *Acta Crystallogr. D Biol. Crystallogr.* **57,** 1373–1382
14. Emsley, P., and Cowtan, K. (2004) *Acta Crystallogr. D Biol. Crystallogr.* **60,** 2126–2132
15. McRee, D. E. (1999) *J. Struct. Biol.* **125,** 156–165
16. Murshudov, G. N., Vagin, A. A., and Dodson, E. J. (1997) *Acta Crystallogr. D Biol. Crystallogr.* **53,** 240–255
17. Otwinowski, Z., and Minor, W. (1997) *Methods Enzymol.* **276,** 307–326
18. Morris, A. L., MacArthur, M. W., Hutchinson, E. G., and Thornton, J. M. (1992) *Proteins* **12,** 345–364
19. Fullerton, S. W., Blaschke, M., Coutard, B., Gebhardt, J., Gorbalenya, A., Canard, B., Tucker, P. A., and Rohayem, J. (2007) *J. Virol.* **81,** 1858–1871
20. Rothwell, P. J., and Waksman, G. (2005) *Adv. Protein Chem.* **71,** 401–440
21. Ng, K. K., Cherney, M. M., Vazquez, A. L., Machin, A., Alonso, J. M., Parra, F., and James, M. N. (2002) *J. Biol. Chem.* **277,** 1381–1387
22. Choi, K. H., Groarke, J. M., Young, D. C., Kuhn, R. J., Smith, J. L., Pevear, D. C., and Rossmann, M. G. (2004) *Proc. Natl. Acad. Sci. U. S. A.* **101,** 4425–4430
23. Biswal, B. K., Cherney, M. M., Wang, M., Chan, L., Yannopoulos, C. G., Bilimoria, D., Nicolas, O., Bedard, J., and James, M. N. (2005) *J. Biol. Chem.* **280,** 18202–18210
24. Gohara, D. W., Crotty, S., Arnold, J. J., Yoder, J. D., Andino, R., and Cameron, C. E. (2000) *J. Biol. Chem.* **275,** 25523–25532
25. Gohara, D. W., Arnold, J. J., and Cameron, C. E. (2004) *Biochemistry* **43,** 5149–5158
26. Korneeva, V. S., and Cameron, C. E. (2007) *J. Biol. Chem.* **282,** 16135–16145
27. Thompson, A. A., Albertini, R. A., and Peersen, O. B. (2007) *J. Mol. Biol.* **366,** 1459–1474
28. Vazquez, A. L., Alonso, J. M., and Parra, F. (2000) *J. Virol.* **74,** 3888–3891
29. Batra, V. K., Beard, W. A., Shock, D. D., Krahn, J. M., Pedersen, L. C., and Wilson, S. H. (2006) *Structure* **14,** 757–766
30. Alberts, I. L., Wang, Y., and Schlick, T. (2007) *J. Am. Chem. Soc.* **129,** 11100–11110
31. Johnson, S. J., Taylor, J. S., and Beese, L. S. (2003) *Proc. Natl. Acad. Sci. U. S. A.* **100,** 3895–3900
32. Doublie, S., Tabor, S., Long, A. M., Richardson, C. C., and Ellenberger, T. (1998) *Nature* **391,** 251–258
33. Li, Y., Korolev, S., and Waksman, G. (1998) *EMBO J.* **17,** 7514–7525
34. Huang, H., Chopra, R., Verdine, G. L., and Harrison, S. C. (1998) *Science* **282,** 1669–1675
35. Beard, W. A., and Wilson, S. H. (2006) *Chem. Rev.* **106,** 361–382
36. Kuchta, R. D., Mizrahi, V., Benkovic, P. A., Johnson, K. A., and Benkovic, S. J. (1987) *Biochemistry* **26,** 8410–8417
37. Arnold, J. J., and Cameron, C. E. (2004) *Biochemistry* **43,** 5126–5137
38. DeLano, W. L. (2002) *The PyMOL Molecular Graphics System*, DeLano Scientific, San Carlos, CA